4.8 AN EVALUATION OF TWO GCMS: NORTH AMERICAN TELECONNECTIONS AND SYNOPTIC PHENOMENA

J.T. Schoof* and S.C. Pryor
Indiana University, Bloomington, Indiana

1. INTRODUCTION

Coupled atmospheric-oceanic global climate models (AOGCMs, or just GCMs) are widely used tools for developing climate prognoses and evaluating climate sensitivities. Because these models have poor spatial resolution (typically $2.5° \times 2.5°$ or worse) and because they exhibit varying skill at different spatio-temporal scales, it is necessary to use downscaling tools (either Regional Climate Models (RCMs) - e.g. Pan et al. (2001), or empirical models - e.g. Wilby et al. (1998)) to derive regional climate prognoses. These tools rely on accurate simulation of synoptic and larger scale climate phenomena in GCMs. If these large-scale features are not simulated realistically within GCMs, the derived downscaled climates will likewise be invalid.

The objectives of this study are thus to evaluate the simulation of the synoptic-scale climate of the Midwestern United States (Figure 1) by HadCM3 (the Hadley Center coupled climate model, version 3: Gordon et al. 2000; Pope et al. 2000) and CGCM2 (the Canadian Centre for Climate Modeling and Analysis coupled climate model, version 2: Flato et al. 2000; Flato and Boer 2001) relative to the NCEP/NCAR reanalysis (NNR) data set (Kalnay et al. 1996; Kistler et al. 2001). This analysis is conducted in terms of three diagnostics: (A) simulation of the probability distributions of large-scale teleconnection indices (the Pacific North American (PNA) index and the North Atlantic Oscillation (NAO) index), (B) nature and frequency of synoptic scale circulations patterns at 500 hPa over the study area, and (C) the relationship between the teleconnection indices and 500-hPa circulation types. The evaluation is conducted for a 'reference period' (1990-2001) relative to the NNR data set, and observed discrepancies between the GCM-derived and NNR data are considered in the context of differences between the NNR data from a historical period (1953-1964) and a future time window as simulated by HadCM3 and CGCM2 (2030-2041). This comparison allows us to determine the confidence with which we can view GCM-simulated prognostic climates for the coming decades by comparing projected changes in teleconnection indices and synoptic scale phenomena with the differences between models and the reanalysis data for the reference period (1990-2001).

2. DATA

The NCEP/NCAR reanalysis (NNR) project combined data from a range of sources in an assimilation scheme to produce temporally continuous "observed" (gridded) atmospheric fields for 1953-2001. In this study, twice-daily 500 hPa geopotential height fields from the NNR are averaged to produce daily fields from which the PNA index and circulation climatology for the study region are derived. Daily NAO indices are computed using daily sea-level pressure values calculated using the hypsometric equation applied to twice-daily NNR surface pressure and 2-m temperature fields and NNR grid point elevation data.

This study uses daily GCM output from two transient simulations for the SRES A2 emissions scenario (IPCC 2000). HadCM3 is a non-flux adjusted GCM with 19 vertical levels and atmospheric grid resolution of $2.5° \times 3.75°$. CGCM2 employs flux adjustments and has 10 vertical levels with atmospheric grid resolution of approximately $3.75° \times 3.75°$. Daily 500 hPa geopotential height and mean sea-level pressure (MSLP) fields from these transient run are available for the period 1990-2099 and are used to evaluate the simulation of teleconnection indices and synoptic-scale climate over the Midwest US (Figure 1) within the GCMs. To further reconcile differences between the NNR, HadCM3, and CGCM2 data sets, all of the fields were linearly interpolated to the NNR grid (Figure 1) using an inverse distance weighted interpolation algorithm.

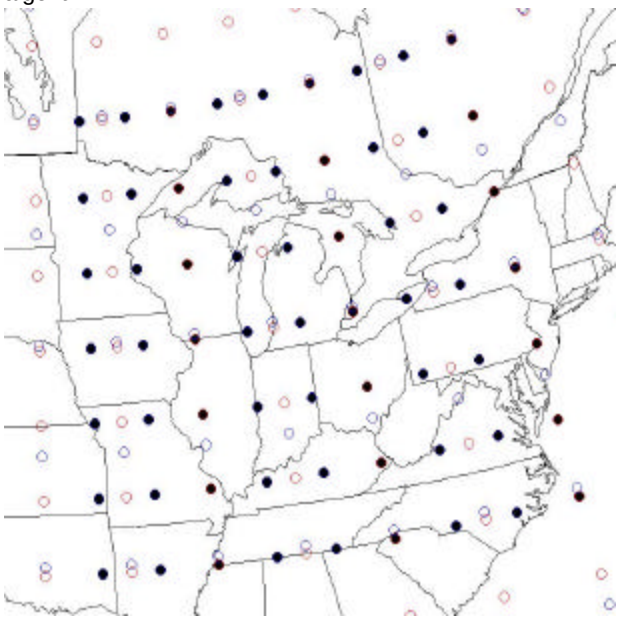

FIGURE 1. Map of study area showing NNR grid points used for Kirchhofer map-type classification (•) and original HadCM3 (o) and CGCM2 (o) grid points.

*_Corresponding author address_: J.T. Schoof, Indiana University, Atmospheric Science Program, Geography, Bloomington, IN 47405; e-mail: jschoof@indiana.edu.

3. METHODS

The study region for this research was chosen primarily because of the importance of climate variability and change for agriculture in the region. The synoptic scale climate of the Midwestern USA is characterized by high-frequency variability associated with both the behavior of the polar jet stream and the relative intensity of several semi-permanent pressure systems. Variations in the intensity of these pressure systems, and the tracking and intensity of synoptic scale phenomena, are in turn controlled by larger pressure oscillations (or teleconnection patterns), particularly the NAO and PNA.

Over the last century, the Upper Great Lakes region has warmed by as much as 2 °C, while parts of the Ohio Valley have cooled by about 0.5 °C. Precipitation has increased throughout the study area due to an increased occurrence of heavy precipitation events. Some of the precipitation changes have been as large as 20% (USNA 2001).

3.1. *Teleconnection indices*

The NAO and PNA indices are typically examined on inter-annual or even inter-decadal timescales (Osborn et al. 1999), but they also exhibit important variability on shorter timescales (Stephenson and Pavan 2003). The comparison of observed (NNR) and GCM-simulated (HadCM3 and CGCM2) teleconnection indices presented here is based on examination of daily indices for the entire calendar year and individual meteorological seasons (winter (DJF), spring (MAM), summer (JJA), and fall (SON)) for 12-year temporal windows as manifest in the NNR data set and simulated by the GCMs.

3.1.1. *The North Atlantic Oscillation (NAO) index*

The North Atlantic Oscillation (Hurrell et al. 2003), is typically characterized by sea-level pressure anomalies associated with the Azores high and the Icelandic low (Lamb and Peppler 1987, Osborn et al. 1999; Hurrell et al. 2003). The positive phase of the NAO (strong Azores high and deep Icelandic low) is generally associated with higher temperatures and increased moisture content in the Midwestern USA (Dickson and Namias 1976; Yarnal and Leathers 1988; Yin 1994).

Simulated NAO time series from a range of GCMs have been shown to reproduce the observed slight serial correlation (Stephenson and Pavan 2003), and Osborn et al. (1999) demonstrated that the previous version of the Hadley Center model (HadCM2) accurately reproduced the spatial patterns of the NAO. However, the teleconnection with the North Pacific in HadCM2 was too strong relative to observations, and periodicities in the simulated time series did not reproduce those present in the observed series. Additionally, GCM derived NAO from several models has been shown to exhibit unrealistic monotonic trends (Stephenson and Pavan 2003).

In this study, the NAO index is computed as the difference in standardized SLP between two NAO "centers of action", at Ponta Delgada, Azores (37.7°N, 25.7°W) and Stykkisholmur, Iceland (65.1°N, 22.7°W). Because NNR and GCM output is not archived at these locations, output from each data source was interpolated to match these coordinates. Calculation of the NAO using monthly standardization within the temporal window under consideration is used here to avoid contamination by long-term trends in the mean pressure patterns since our focus is on the range and variability of the daily NAO and PNA across a number of temporal windows.

3.1.2. *The Pacific-North American (PNA) index*

The mean flow over the Pacific-North American sector is characterized by a trough in the east-central North Pacific, a ridge over the Rocky Mountains, and a trough over eastern North America (Leathers et al. 1991). The PNA teleconnection index reflects deviations from this mean flow, suggesting more meridional (positive phase) or zonal (negative phase) flow over North America. The PNA is closely linked to both thermal and hydrologic regimes within the Midwestern USA (e.g., Coleman and Rodgers 2003; Sheridan 2003; Leathers et al. 1991; Yin 1994; Henderson and Robinson 1994).

Relative to the NAO, comparatively few studies have quantified the ability of GCMs to accurately simulate the PNA. Renshaw et al. (1998) showed that HadAM3, the atmospheric component of HadCM3, correctly reproduces the changes in the frequency distribution of the PNA index associated with the phases of ENSO, although Kang et al. (2002) showed that several atmospheric GCMs underestimated the amplitude of the PNA pattern associated with the 1997-98 El Niño event.

The PNA index used in this study is computed using the equation of Wallace and Gutzler (1981):

$$PNA = \frac{1}{4}\left[\begin{array}{l} Z(20^\circ N, 160^\circ W) - Z(45^\circ N, 165^\circ W) \\ + Z(55^\circ N, 115^\circ W) - Z(30^\circ N, 85^\circ W) \end{array}\right] \quad (1)$$

where Z are standardized (by month within the study period) 500 hPa geopotential height values. As with the NAO, the GCM-simulated PNA index is obtained by interpolating the HadCM3 and CGCM2 data to match the grid points given in Equation (1).

3.1.3. *Evaluation of large-scale teleconnection indices*

For each GCM, we evaluate the teleconnection indices by comparing observed and simulated empirical cumulative distribution functions (ECDFs) using the Kolmogorov-Smirnov (K-S) test (Wilks, 1995). The test is conducted under the null hypothesis that the daily teleconnection indices are drawn from the same, unspecified distribution. The K-S test statistic is the largest absolute difference between observed and simulated ECDFs. The observed and simulated teleconnection indices are also compared in terms of

the temporal behavior of the daily values using the partial autocorrelation function (PACF), which represents the autocorrelation at a particular lag in a time series that is not accounted for by autocorrelation at previous lags. In this way, we evaluate the model's ability to simulate both the probability distributions and the temporal behavior of the teleconnection indices.

3.2. *Synoptic-scale map-pattern analysis*

Relatively few studies have focused on evaluation of GCMs at the synoptic scale and those that have indicate the model performance is both regionally and seasonally variable (e.g., Schubert 1998; Lapp et al. 2002; Katzfey and McInnes 1996; McKendry et al. 1995).

3.2.1. *Map-typing*

Here we use the correlation-based method of Kirchhofer (1974) to classify 500 hPa fields from NNR and the GCMs. The Kirchhofer score of similarity, S, for two grid-point maps, containing x and y, is given by:

$$S = \sum_{i=1}^{n} (z_{xi} - z_{yi})^2 \qquad (2)$$

In Equation (2), z_{xi} and z_{yi} are the normalized grid-point values of x and y, respectively, and s_x and s_y are the standard deviations of x and y, respectively. Normalization of the data ensures that the value of S indicates similarity in map patterns and is not contaminated by the magnitudes of the values being classified (Blair, 1998). Wilmott (1987) provided a simple relationship between the Kirchhofer score, S, and the coefficient, r:

$$Sn^{-1} = 2[1 - r(x,y)] \text{ , } 0 \le Sn^{-1} \le 4 \qquad (3)$$

We follow the suggestion of Blair (1998) by using n-1 in place of n in Equation 3. By setting a threshold for the required correlation, Equation 3 can be used to determine the appropriate threshold for S. Subjectivity in the application of the Kirchhofer method arises due to the need to set a threshold for similarity and a minimum group size (Yarnal 1985; McKendry et al. 1995). In this study, the correlation threshold is set at 0.55 and the map-pattern groups are required have more than six members. These values are chosen to ensure a manageable number of weather types and a high percentage of classified days.

3.2.2. *Evaluation of synoptic-scale map-pattern classification*

In this study we apply the Kirchhofer method to the 1990-2001 NNR 500 hPa geopotential heights fields. We then apply 'targeted' Kirchhofer classifications to HadCM3 and CGCM2 output for the 1990-2001 period, the 1953-1964 NNR data and 2030-2041 HadCM3 and CGCM2 fields. In each targeted classification, the key days identified in the 1990-2001 NNR are used as seeds. Days meeting the similarity threshold with one of the established keydays are removed from the analysis along with all days that are similar to them. Once all observations have been compared to all keydays a second run through the data allows reassignment of previously classified observations. Use of the targeted classifications facilitates quantitative comparisons of the 'base' classification for the reference period (1990-2001) and those from a historical and future period to determine whether differences in the synoptic regimes as manifest the NNR and GCM time series exceed those due to climate evolution.

The comparison of the synoptic classifications for the different time series is based on the annual and seasonal means and standard deviations of the map type frequencies. Thus, the results of the analysis provide a measure of the similarity in observed and simulated interannual climate variability (with n=12). The equality of the means of the frequencies is tested using the Student's t-test for the case of assumed unequal variances, with degrees of freedom estimated using the Satterthwaite approximation (Satterthwaite, 1946). The null hypothesis for this test is that there is no difference in the observed and simulated mean map-type frequencies. To test the equality of the variances of the map-type frequencies, the standard F statistic is employed on the basis of the standard deviations of seasonal frequencies. Both of these statistical tests are based on assumptions about the underlying samples. In particular, the observations in each sample are assumed to be independent, to exhibit a near normal distribution, and the frequencies within one sample are assumed to be independent of those in other samples. Because the sample sizes associated with most map-types are large, deviations from normality are not expected to have a large impact on the results. For map-types that occur less frequently, the inferences made on the basis of these tests should be treated with more caution.

In addition to the annual and seasonal individual map-type frequencies, the analysis of the synoptic scale map-types also includes an examination of the persistence of individual map patterns and the progression from one map pattern to another, as well as a chi-squared test for the agreement of the entire distribution of synoptic map-types on annual and seasonal timescales.

3.3. *Relationships between teleconnections and Midwest US map-types*

For each season and for the entire year, the frequency of each weather type is determined for each phase of the NAO and PNA. A positive day for each teleconnection is defined as a day when the teleconnection is at least one standard deviation above the mean for the season in question. Similarly, a negative day occurs when the teleconnection is at least one standard deviation below the mean.

To quantify variations in the links between the teleconnection indices and the weather types on an annual and seasonal basis a two-sample difference of proportions test (Ott, 1993; Sheridan 2003) is applied to

the teleconnection phase scores. In this analysis the two proportions are compared with a z-score:

$$z = \frac{p_1 - p_2}{\hat{s}} \quad (4)$$

where π_1 and π_2 represent the proportions of positive and negative phase days for a particular season, Kirchhofer weather type, and teleconnection, and $\hat{s}$ is:

$$\hat{s} = \sqrt{\hat{p}(1-\hat{p})\left(\frac{1}{n_1} + \frac{1}{n_2}\right)} \quad (5)$$

where n_1 and n_2 are the total number of days in the season of the positive NAO or PNA phase and negative NAO or PNA phase, respectively, and $\hat{p}$ is

$$\hat{p} = \frac{n_1 p_1 + n_2 p_2}{n_1 + n_2} \quad (6)$$

The test is not performed for weather types for which $n\hat{p}$ or $n(1-\hat{p})$ is less than 5 for either proportion because the normal approximation to the binomial does not hold for small sample sizes.

4. RESULTS

4.1. *Teleconnection indices*

4.1.1. *North Atlantic Oscillation (NAO)*

When the ECDFs of daily NNR, HadCM3, and CGCM2 NAO indices are compared for the reference period (1990-2001), the null hypothesis that the observed and simulated NAO indices are drawn from the same underlying distribution cannot be rejected at the α = 0.05 level (Table 1) for either GCM. Additionally, analyses on the individual seasons suggest that differences in the seasonal distributions are not significant.

Comparison of partial autocorrelation functions (PACFs) indicates that the observed and simulated NAO indices are also similar in terms of their temporal autocorrelation (Figure 2a). The slight underestimation of the magnitude of the partial autocorrelation at lags greater than one by the GCMs is consistent with slightly stronger autocorrelation of the NAO index within the models.

In short, the statistical evaluation performed here suggests that both HadCM3 and CGCM2 capture the major features of the observed distribution and temporal behavior of the daily NAO index as manifest in the NNR.

Analysis of the NAO index from the 1953-1964 NNR data suggests excellent agreement with the 1990-2001 index in terms of both the distribution and PACF of the normalized index (Table 1, Figure 2a). On both annual and season timescales, we are unable to reject the null hypothesis that NNR 1990-2001 and NNR 1953-1964 are drawn from the same underlying distribution. This implies that the established underlying trend in the north-south pressure difference in the Atlantic in the latter portion of the twentieth century (Pryor and Barthelmie, 2003) was not accompanied by an increase in variability.

In keeping with the NNR derived historical period, a comparison of the ECDFs of the 1990-2001 and 2030-2041 HadCM3 and CGCM2 NAO indices also suggests that the probability distribution of the NAO will not change drastically over the approaching decades. The results of this analysis thus indicate that the distribution of NAO index values and their temporal behavior are well-simulated by both GCMs and that the variability of the pressure gradient across the Atlantic will not evolve greatly over the next three decades.

Table 1. Results of K-S tests performed on NNR and HadCM3 NAO and PNA indices. For each season the table provides the K-S statistic and p-value (i.e., the probability of observing a difference as extreme as or more extreme than the observed difference if the null hypothesis is true) associated with the test. Table entries are underlined if statistically significant at α=0.05.

	NNR vs. HadCM3 1990-2001		**NNR vs. CGCM2 1990-2001**	
	NAO	PNA	NAO	PNA
ANN	0.0146 (0.7388)	0.0255 (0.2166)	0.0184 (0.4458)	0.0240 (0.1565)
DJF	0.0406 (0.3267)	0.0664 (0.0158)	0.0356 (0.4885)	0.0638 (0.0228)
MAM	0.0270 (0.8176)	0.0352 (0.4995)	0.0317 (0.6292)	0.0362 (0.4566)
JJA	0.0284 (0.7635)	0.0199 (0.9806)	0.0299 (0.7012)	0.0199 (0.9797)
SON	0.0213 (0.9655)	0.0537 (0.0858)	0.0484 (0.1528)	0.0670 (0.0145)
	NNR 1990-2001 vs. NNR 1953-1964		**NNR 1990-2001 vs. NNR 1953-1964**	
	NAO		PNA	
ANN	0.0187 (0.4237)		0.0205 (0.3109)	
DJF	0.0384 (0.3896)		0.0374 (0.4198)	
MAM	0.0245 (0.8924)		0.0589 (0.0418)	
JJA	0.0236 (0.9164)		0.0281 (0.7713)	
SON	0.0361 (0.4750)		0.0185 (0.9920)	
	HadCM3 1990-2001 vs. HadCM3 2030-2041		**CGCM2 1990-2001 vs. CGCM2 2030-2041**	
	NAO	PNA	NAO	PNA
ANN	0.0123 (0.8994)	0.0104 (0.9725)	0.0176 (0.5043)	0.0219 (0.2408)
DJF	0.0324 (0.6152)	0.0204 (0.9773)	0.0500 (0.1305)	0.0407 (0.3253)
MAM	0.0176 (0.9959)	0.0370 (0.4424)	0.0335 (0.5579)	0.0263 (0.8361)
JJA	0.0333 (0.5791)	0.0324 (0.6152)	0.0272 (0.8045)	0.0380 (0.3947)
SON	0.0259 (0.8566)	0.0343 (0.5435)	0.0293 (0.7305)	0.0421 (0.2814)

4.1.2. *Pacific/North American (PNA) index*

The null hypothesis that NNR and GCM-simulated PNA indices are drawn from the same underlying distribution also cannot be rejected on the annual timescale. At the seasonal timescale, the null hypothesis is rejected for the winter season (both GCMs) and for the fall season (CGCM2 only) (Table 1). Interestingly, the differences in the distributions for

these seasons do not occur near the tails. As shown in Figure 3, differences in observed and simulated PNA index distributions result from differences in skewness (winter; Figure 3a, b) and kurtosis (fall; Figure 3c). Figure 2b shows that the partial autocorrelation function of the simulated PNA index is in good agreement with observations.

Daily PNA indices calculated from the NNR data for 1953-1964 and 1990-2001 suggest that there is only evidence to reject the null hypothesis of similar underlying probability distributions during spring (Table 1). Figure 3d shows that during the spring the 1953-1964 and 1990-2001 PNA indices differ in terms of kurtosis. The partial autocorrelation functions for the PNA index during these periods (Figure 2b) are similar in magnitude and sign.

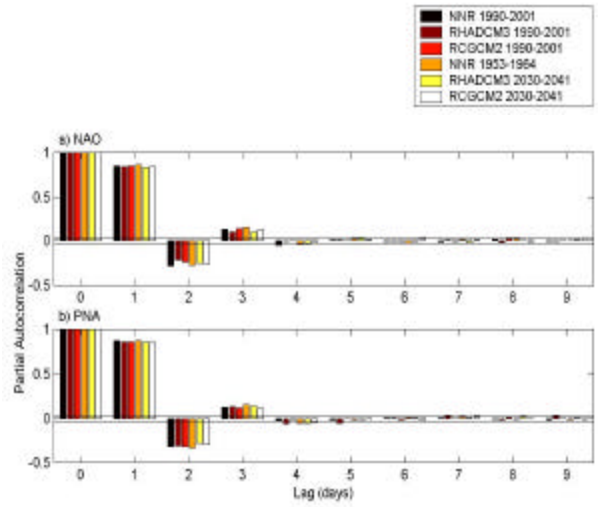

Figure 2. Partial autocorrelation functions for observed and simulated (a) NAO and (b) PNA time series. The horizontal lines separate statistically significant autocorrelations from those expected from a random process.

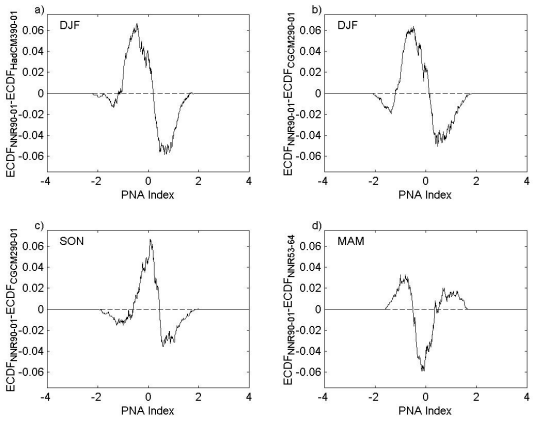

Figure 3. Differences between empirical cumulative distribution functions (ECDFs) of the PNA index for a) NNR-HadCM3 1990-2001 DJF, b) NNR-CGCM2 1990-2001 DJF, c) NNR-CGCM2 1990-2001 SON, and d) NNR 1990-2001-NNR 1953-1964 MAM.

A comparison of the empirical distribution functions of the 1990-2001 and 2030-2041 PNA index derived from HadCM3 and CGCM2 also indicates close accord between the reference and future periods. For each season, and annually, we are unable to reject the null hypothesis that these two distributions are drawn from the same distribution (Table 1). The partial autocorrelation functions (Figure 2b) display a level of agreement similar to the reference period observed and modeled series, suggesting that there is a lack of evidence for a coming change in the distribution and serial correlation of the PNA at the daily timescale.

4.1.3. *Summary*

The results presented in Sections 4.1.1 and 4.1.2 indicate that HadCM3 and CGCM2 capture the distribution and temporal evolution of the daily NAO and PNA indices. These analyses focus on shorter time scales (primarily sub-annual) and are conducted over shorter temporal windows than those of previous studies (e.g., Osborn et al. 1999; Stephenson and Pavan 2003) and hence the results should not be interpreted as implying agreement in terms of long-term trends or variations. In addition, our station-based calculations of normalized teleconnection indices are not designed to capture changes in the location of the major NAO and PNA centers of action or a linear trend in the pressure gradients. An important note in light of the analysis of HadCM2 by Osborn et al. (1999) who found the NAO index was too strongly correlated to Pacific Ocean SLP anomalies, the daily NAO and PNA indices calculated from HadCM3, CGCM2 and NNR data for 1990-2001 are only weakly correlated (< |0.04| for NNR and HadCM3, < |0.08| for CGCM2).

4.2. Synoptic-scale map pattern analysis

4.2.1. *Observed map patterns: 1990-2001.*

When applied to the 1990-2001 daily NNR 500-hPa geopotential height fields, the Kirchhofer method (Section 3.2.1) identifies 20 map patterns accounting for 89% of the observations. Figure 4 shows the mean fractional seasonal frequency for each type while Table 2 shows persistence of each type (2a), and progression of the types (2b). For all types and all data sets the class correlations greatly exceed the threshold of 0.55 (all exceed 0.85) suggesting these classifications are robust (i.e. the 'types' are internally coherent). Correlations between the mean Kirchhofer map-type fields as manifest in the NNR and each GCM exceed 0.97 for each of the first 15 map-types.

The first Kirchhofer map pattern typically represents the "average" pattern. This pattern accounts for 17.1% of the observations and is characterized by zonal flow and a trough located north/northeast of the study area. A ridge located to the east/southeast and southwesterly

flow over the study area characterizes the second most prevalent pattern identified by the analysis, which accounts for 13.6% of the observations. With the exception of pattern twelve (12%), each of the subsequent patterns accounts for less than 10% of the observations, although each represents a unique and meaningful synoptic-scale flow regime.

a)

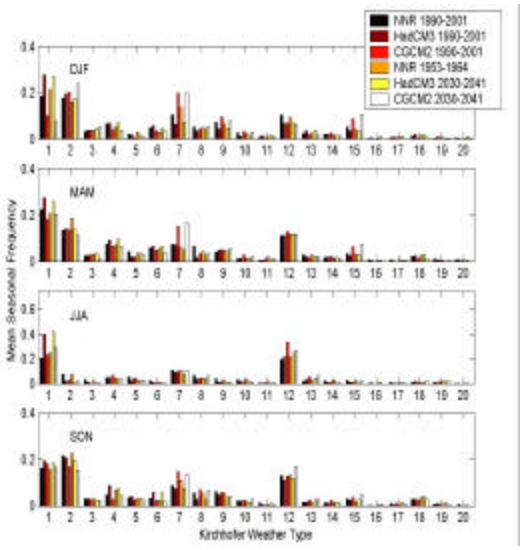

b)

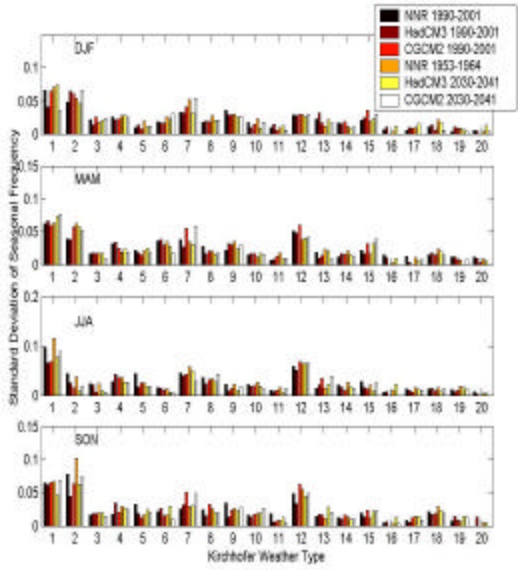

Figure 4. Means (a) and standard deviations (b) of seasonal frequencies for the 20 Kirchhofer map-types as observed (NNR) and simulated by HadCM3 and CGCM2.

4.2.2. *Comparison of NNR and transient GCMs for the reference period: 1990-2001*

The targeted Kirchhofer analysis of the HadCM3 and CGCM2 simulations for 1990-2001 led to classification of 90.8% and 91.7% of simulated days, respectively. The GCM-based classifications are similar to the NNR classification in terms of the mean correlation coefficients and persistence (Table 2) for each of the map-types. In addition, the models correctly simulate the progression of nearly all of the map-types (and particularly the most common types). While the map-type frequencies are generally similar, the most common map-type occurs far too often in HadCM3 and slightly too seldom in CGCM2 relative the observed record (Table 2).

Comparison of the observed and simulated map-types on a seasonal basis (Figure 4) shows that both HadCM3 and CGCM2 simulations adequately simulates the seasonality of the map-type frequencies for most of the map-types identified in the NNR. Overestimation of the first map-type by HadCM3 is largest during the summer and winter months, with only slight overestimation during the transition seasons. During the summer months, the overestimation of the first map-type by HadCM3 also results in an underestimation of several subsequent map-types (Figure 4a).

Table 2 Mean persistence (a) and most commonly preceding map-types (b) for each of the Kirchhofer map-types identified from the NNR, HadCM3, and CGCM2 500-hPa geopotential height fields. Persistence is determined by examining all runs of each map-pattern within the observed data and is defined as the average run length. Map-pattern progression is examined by recording which map types most frequently precede each other.

a) Mean Persistence

	NNR 1990-2001	Had 1990-2001	CGCM 1990-2001	NNR 1953-1964	Had 2030-2041	CGCM 2030-2041
1	1.793	2.250	1.768	2.003	2.269	1.861
2	1.624	1.808	1.642	1.778	1.766	1.764
3	1.178	1.117	1.084	1.094	1.020	1.025
4	1.114	1.197	1.110	1.168	1.161	1.068
5	1.195	1.065	1.076	1.144	1.082	1.048
6	1.075	1.139	1.069	1.054	1.107	1.047
7	1.240	1.225	1.345	1.331	1.180	1.312
8	1.128	1.073	1.129	1.117	1.126	1.140
9	1.138	1.079	1.076	1.071	1.047	1.117
10	1.128	1.052	1.054	1.197	1.070	1.117
11	1.035	1.136	1.053	1.163	1.091	1.046
12	1.454	1.438	1.624	1.482	1.521	1.476
13	1.123	1.129	1.129	1.149	1.255	1.154
14	1.029	1.068	1.068	1.085	1.125	1.048
15	1.110	1.095	1.155	1.048	1.103	1.200
16	1.556	1.286		1.000	1.385	1.000
17	1.033	1.071	1.000	1.074	1.061	1.200
18	1.086	1.082	1.087	1.149	1.145	1.119
19	1.077	1.192	1.040	1.067	1.063	1.039
20	1.200	1.143	1.000	1.000	1.333	1.000

b) Most Commonly Preceding Types

	NNR 1990-2001	**HadCM3 1990-2001**	**CGCM 1990-2001**
1	1,7,12	1,7,12	1,7,12
2	2,6,4	2,6,4	2,6,4
3	2,9,3	2,9,3	2,9,3
4	12,1,4	12,1,4	12,1,4
5	1,12,4	1,12,4	1,0,12
6	4,12,0	4,12,1	4,15,12
7	7,2,8	7,2,9	7,0,9
8	2,8,0	2,0,12	2,0,8
9	2,9,15	2,4,9	2,0,6
10	0,10,12	4,2,12	0,12,7
11	1,0,7	1,7,3	7,1,8
12	12,2,7	12,1,7	12,1,7
13	1,8,0	1,13,2	1,7,8
14	4,7,10	12,4,0	9,0,12
15	2,9,12	2,9,12	9,2,0
16	0,16,1	1,16,0	
17	0,2,7	2,5,6	0,2,3
18	5,0,12	5,12,0	0,5,1
19	2,0,5	2,5,13	0,12,1
20	4,2,20	12,20,4	12
	NNR 1953-1964	**HadCM3 2030-2041**	**CGCM 2030-2041**
1	1,7,12	1,7,12	1,7,12
2	2,4,6	2,6,4	2,6,4
3	2,9,3	2,9,16	2,9,16
4	12,1,4	12,1,4	12,7,1
5	1,12,4	1,12,4	1,12,7
6	4,12,0	4,12,1	4,15,12
7	7,1,9	7,2,9	7,0,15
8	2,0,8	2,8,0	2,7,8
9	2,12,0	2,6,4	2,9,15
10	10,0,12	12,0,1	0,12,2
11	1,11,3	1,3,7	1,7,0
12	12,1,7	12,1,0	12,1,0
13	8,0,1	1,13,0	0,13,8
14	7,12,4	12,15,4	7,12,15
15	2,9,12	2,12,9	15,2,0
16	0,1	1,16,0	1
17	0,2,15	2,6,0	2,0,17
18	5,0,18	4,1,18	0,4,12
19	0,1,12	1,16,7	1,11,12
20	0,1,4	4,6,10	0

The underestimation of the first map-type by CGCM2 is mostly confined to the winter, with slight underestimation also occurring during spring. CGCM2 also over-simulates the mean annual frequency of map-type 7, especially during winter, but also during the transition seasons. The standard deviations of the seasonal frequencies (Figure 4b) suggest that the GCMs also underestimate the interannual variability of the first map-type during winter (HadCM3) and summer (HadCM3 and CGCM2).

Application of the student t-test (Table 3) confirms that the mean annual frequencies of eight HadCM3 and nine CGCM2 map-types are significantly different in the GCM simulations for the reference period compared to the NNR , including the first (and most common) map-type in HadCM3. The seasonal results suggest that these differences are primarily due to differences within one or two seasons. For example, the differences in mean frequency of HadCM3 map-type 4 can be attributed to the fall months, while the frequencies are similar to those in the NNR in other seasons. Similarly, those for CGCM2 map-type 4 can be attributed to the fall and winter months.

Table 3. Results of application of the student's T-test and the F-test to examine differences in means and standard deviations of map-type frequencies from the NNR and HadCM3 (a) and CGCM2 (b) SRES A2 simulation for the entire year and by season for 1990-2001. The table shows the statistic (t-statistic for the "mean test" and F-statistic for the "variance test") associated with the test. Table entries are underlined if statistically significant at α=0.05. A blank means that the test was not performed because the map-type (in either analysis) does not occur within the season.

a) HadCM3

Map-type	Mean Test				
	ANN	DJF	MAM	JJA	SON
1	-5.57	-4.02	-1.98	-5.80	-1.28
2	1.00	-0.74	-0.57	3.70	0.48
3	0.80	-0.88	0.34	2.11	-0.05
4	-3.65	-0.25	-1.20	-0.19	-3.43
5	2.29	-0.52	2.71	2.29	-0.42
6	-1.27	-1.02	-0.42	1.43	-2.69
7	2.89	2.92	0.13	1.04	1.11
8	6.82	2.20	5.23	2.37	3.41
9	2.36	2.16	-0.71	3.50	1.17
10	1.87			1.86	-0.23
11	0.64				
12	0.87	2.88	-0.01	-0.90	1.34
13	-1.53	-0.79	1.07	-2.55	-0.08
14	0.52	0.22	-0.64	1.19	
15	2.86	1.78	0.98		1.07
16	-0.46				
17	2.53				
18	-1.14	-1.47	-0.33	-0.58	-0.08
19	-0.11				
20					
Map-type	Variance Test				
	ANN	DJF	MAM	JJA	SON
1	1.45	2.58	0.88	2.22	1.10
2	1.37	0.56	1.08	2.87	2.90
3	1.60	2.59	0.95	1.31	0.81
4	0.33	1.37	0.87	0.41	*0.26*
5	2.60	0.49	1.39	6.10	2.95
6	0.73	1.17	0.93	1.14	0.67
7	1.39	1.11	2.09	1.24	0.69
8	2.43	0.76	2.77	2.40	2.39
9	1.69	1.58	0.46	6.09	6.73
10	2.20			1.65	1.49
11	1.13				
12	0.44	1.03	1.13	1.72	2.12
13	0.47	0.52	3.56	1.35	0.72
14	1.45	1.23	0.52	0.50	
15	2.60	0.70	1.66		1.98
16	0.85				
17	1.37				
18	0.62	0.67	0.70	0.90	1.42
19	0.49				
20					

b) CGCM2

Map-type	Mean Test				
	ANN	DJF	MAM	JJA	SON
1	1.20	3.20	1.75	-0.71	-0.88
2	1.38	-1.19	-0.20	3.96	1.75
3	1.76	-0.56	-0.10		0.62
4	2.27	2.37	0.70	-1.59	2.50
5	2.96		2.96	0.69	1.06
6	2.39	1.84	0.89		1.66
7	-6.61	-6.19	-4.05	0.61	-3.57
8	2.55	1.21	3.27	2.03	-0.93
9	-0.47	-1.76	-0.87	2.80	0.08
10	-0.74	-0.86		1.60	-0.48
11	1.07				
12	-2.76	2.79	-0.67	-5.41	0.20
13	-1.90	0.69	1.43	-3.34	-1.04
14	-0.88	-0.81	-0.88		
15	-2.65	-3.06	-2.76	1.84	-0.68
16					
17	2.27				
18	2.23				0.20
19	0.17				
20					
Map-type	Variance Test				
	ANN	DJF	MAM	JJA	SON
1	1.19	1.04	1.09	2.05	0.95
2	0.59	0.62	0.47	7.52	1.47
3	4.56	0.70	1.06		0.83
4	0.75	1.32	1.60	0.60	0.71
5	4.51		2.03	3.05	6.95
6	2.61	1.21	1.44		1.88
7	0.50	0.65	0.48	1.10	0.26
8	0.73	0.90	1.87	1.26	0.56
9	1.51	1.58	0.54	2.72	2.17
10	1.72	1.31		1.43	0.92
11	0.95				
12	0.34	0.92	0.72	0.76	0.63
13	0.49	1.98	2.10	0.18	0.84
14	3.01	0.81	0.59		
15	0.87	0.33	0.45	4.88	0.70
16					
17	1.04				
18	0.80				1.33
19	2.16				
20					

Seasonal tabulation suggests that both GCMs better replicate the mean annual frequency and inter-annual variability of map-type frequencies during the transition seasons, with poorer performance during the summer and winter. While there is agreement between some of the individual NNR, HadCM3, and CGCM2 map-types, a chi-squared ($?^2$) test confirms that there are significant differences between NNR and each of the GCMs (Table 4) largely as a result of overestimation of a single map-type by the GCM (e.g., map-type 1 in HadCM3, map-type 7 in CGCM2).

4.2.3. *Historical map-type frequencies in NNR: 1953-1964*

As shown in Table 2, the map-type persistence and progression for the 1953-1964 map-types derived from the NNR data record are similar to those for the 1990-2001 map-types. Comparison of the observed map-types on a seasonal basis (Figure 4) shows that each of the map-types identified in the 1990-2001 classification are also present in the earlier 1953-1964 period. The mean annual frequencies in 1953-1964 are only statistically different from those in 1990-2001 for two of the map types (types 8 and 11). On a seasonal basis, the mean frequencies are only significantly different for map-type 6 in the winter, map-types 2 and 8 during the spring and map-type 15 during the fall. The standard deviations of annual frequencies between the two observed classifications are statistically different only for map-type 18, which accounts for less than 2% of the data. Significant differences in the standard deviations of map-type frequencies are found in all seasons except spring (map-types 5, 13, and 18 during winter, type 14 during summer, and type 5 during fall), although it should be noted that the map types for which statistically significant differences exist generally account for a small percentage of the observations (Table 2a).

Table 4. Results of chi-squared ($?^2$) tests performed on NNR, HadCM3 and CGCM2 map-type distributions. For each season the table provides the value of the $?^2$ statistic and p-value (i.e., the probability of observing differences as extreme or more extreme than that observed if the null hypothesis is true) associated with the test. Table entries are underlined if statistically significant at α=0.05.

	NNR vs. HadCM3 1990-2001	**NNR vs. CGCM2 1990-2001**
ANN	179.50 (0.00)	142.13 (0.00)
DJF	71.51 (0.00)	106.44 (0.00)
MAM	53.46 (0.00)	81.35 (0.00)
JJA	159.54 (0.00)	147.55 (0.00)
SON	45.29 (0.00)	46.93 (0.00)
	NNR 1990-2001 vs. NNR 1953-1964	
ANN	34.06 (0.04)	
DJF	26.15 (0.25)	
MAM	33.63 (0.04)	
JJA	30.89 (0.08)	
SON	17.29 (0.86)	
	HadCM3 1990-2001 vs. HadCM3 2030-2041	**CGCM2 1990-2001 vs. CGCM2 2030-2041**
ANN	28.74 (0.14)	29.83 (0.11)
DJF	16.55 (0.76)	21.00 (0.67)
MAM	20.81 (0.69)	18.58 (0.97)
JJA	36.15 (0.02)	45.70 (0.00)
SON	25.44 (0.29)	23.53 (0.43)

4.2.4. *Prognostic map-type frequencies in GCM simulations: 2030-2041*

Eighty-seven percent of both HadCM3 and CGCM2 simulation days for 2031-2040 can be attributed to one of the 20 types identified from analysis of NNR data from 1990-2001. With the exception of map-type 18 during the summer, statistical significance tests indicate the mean annual and seasonal frequencies of map type occurrence in the HadCM3 simulations for 1990-2001 and 2030-2041 are not statistically significant. For

CGCM2, there are significant differences for map-type 14 annually, map-type 3 during the spring, and map-types 12 and 18 during the summer. Annually, the standard deviations of map-type frequencies are also similar to those in the reference period. Nineteen of the twenty total HadCM3 map-types do not show statistically significant differences in the standard deviation of map-type frequencies on the annual timescale. For CGCM2, there are not statistically significant differences for any of the map types tested. The map-types do, however, differ in terms of the interannual variability in the seasonal map-type frequencies (Figure 4). For each season, at least one (and up to three during summer) HadCM3 map-types exhibit statistically significant differences in the variance of map-type frequency. For CGCM2, statistically significant differences in the variance of seasonal map-type frequency were found for map-types 1, 6, and 19 during winter, map-type 3 during the spring, and map-types 6 and 15 during the summer. Application of a $?^2$ test to the 1990-2001 and 2030-2041 HadCM3 and CGCM2 map-type distributions reveals significant differences only for summer (Table 4).

4.2.5. *Summary*

Synoptic scale phenomena as simulated by HadCM3 and CGCM2 for 1900-2001 show a high degree of correspondence with those manifest in the NNR in terms of frequencies, persistence and progression. However, both GCMs appear to underestimate the variability of the synoptic climate and particularly the first few (and most common) Kirchhofer weather-types. The inference that can be drawn from the analysis presented above is that the evolution of synoptic-scale climate over the next 30 years, as characterized by 500-hPa geopotential heights as manifest in the HadCM3 and CGCM2, is smaller than the discrepancy between the observed and CGM-derived synoptic-scale climate for the 1990-2001 reference period.

4.3. Relationships between teleconnection indices and map-type frequencies

Significant differences in map-type frequency with NAO phase (Section 3.3) were not found in the analysis of 1990-2001 NNR. While significant links were not found in CGCM2, HadCM3 map-type 1 exhibits a statistically significant link to NAO phase during winter. The statistical significance of this map-type in HadCM3 may be due to its large sample size relative to its counterparts in the NNR and CGCM2 classifications (see Figure 4).

Unlike the NAO, the PNA was found to be strongly linked to synoptic scale climate in the study area in both the NNR and GCM data from 1990-2001. In the NNR data, five types display statistically significant links to the PNA phase on an annual basis (map-types 1, 2, 3, 4, and 7). On a seasonal basis, fewer NNR map-types exhibit statistically significant links to the PNA. These links predominately occur during the winter (map-types 1, 2, and 9) and also during the fall (map-type 1). HadCM3 also produces several map-types with significant links to the PNA on annual timescales (map-types 1, 2, 4, 5, 7, and 18). As with NNR, there are fewer maps corresponding to particular PNA phase during individual seasons – only two during the winter (map-types 1 and 2) and one during spring (map-type 2). In CGCM2, only four map-types exhibit statistically significant links to the PNA annually (map-types 1, 2, 3, and 7). Seasonally, significant links are found during winter (map-types 1, 2, and 7) and during fall (map-types 2 and 7). While NNR, HadCM3, and CGCM2 map-types show statistically significant links with the PNA, the correspondence by map type is imperfect.

The differences in the significance of the links between the PNA and synoptic map-types can be used to explain some, but not all, of the deficiencies in map-type frequency reproduction within the GCMs. For example, map-type 9 is significantly linked to the PNA in the NNR 1990-2001 DJF data, while a lack of such a relationship in HadCM3 may explain the significant differences in mean map-type frequency for this map-type in HadCM3 relative to NNR. Similarly, map-type 4 is linked to the PNA phase in NNR, while a lack of such a link in CGCM2 may result in the statistically significant differences in the mean map-type frequencies for this map-type.

There is also evidence that the links between the PNA index phase and synoptic types are particularly useful for explaining differences between the GCMs and NNR. For example, the annual and seasonal mean frequencies of HadCM3 map-type 8 are significantly different from those found in NNR (Table 3). While the difference in proportions test does not suggest significant links between the PNA and map-type 8, the map-type is more than twice as likely during the positive phase of the PNA within the NNR. In HadCM3, however, this link is not present and map-type 8 is only slightly more likely during the positive PNA phase. This is also true of several other map-types which are not well-simulated by the GCMs.

5. CONCLUDING REMARKS

Reliable regional climate projections for the mid-latitudes are critically dependent on the accuracy of the depiction of teleconnection indices and synoptic scale phenomena within GCMs. We have presented an evaluation of the synoptic-scale climate of the Midwest region of the United States as manifest in the transient HadCM3 and CGCM2 simulations for the A2 emission scenario relative to the NNR data set.

The probability distribution of the NAO teleconnection index in the reference period (1990-2001) was found to be well simulated on sub-annual timescales, as is the serial correlation of daily NAO. Differences in the distribution of the PNA teleconnection index were found in both HadCM3 (winter only) and CGCM2 (winter and fall). Both GCMs successfully reproduces the range of synoptic-scale map-patterns over the Midwestern USA as manifest in 500 hPa height

fields. Modeled map-types from HadCM3 and CGCM2 are similar to those derived for the NNR data in terms of correlation coefficients, frequency, persistence, and progression. However, the most common map-type occurs more often in the HadCM3 simulation and less often in CGCM2 relative to the NNR, possibly suggesting that the GCMs do not properly capture the total variability in the synoptic-scale circulation. This statement is further supported by spectral analysis of the NNR, HadCM3, and CGCM2 500-hPa fields at coincident points, which suggests that the magnitude of the annual cycle is underestimated by both GCMs in the northern part of the study area.

In both the GCM simulations and NNR data, the NAO was found to exert considerably less influence on map-type frequency in the Midwest than the PNA, which exhibits statistically significant links to multiple Kirchhofer-map type frequencies in both the NNR and GCM time series for 1990-2001. Climate projections for 2030-2041 as generated using HadCM3 and CGCM2 indicate relative stability of the teleconnection indices and synoptic type frequencies in the Midwestern USA on annual and seasonal scales relative to the base period of 1990-2001, although the inter-annual variability of many of the synoptic types is increased relative to the 1990s.

Despite the relatively good correspondence between NNR and these two GCMs with respect to the synoptic climate of the Midwest and the teleconnection indices, differences between the GCMs and NNR in the reference period (1990-2001) are demonstrated to be of comparable or greater magnitude than changes in synoptic types and the teleconnection indices in the GCM simulations for 2030-2041 relative to 1990-2001. The inference that must be drawn from this analysis is that GCM-derived prognoses for the near-term synoptic climate of this region remain uncertain. It is important to note there are four major caveats to this finding. First, there is an implicit assumption that the NNR data series accurately represents the teleconnection indices and synoptic regime of the Midwestern USA, and that the 500-hPa height field is adequate to represent the major features of the synoptic climate. Second, we examined 12-year time windows to ensure direct comparability with the overlap (reference) period for NNR and the GCMs. However, these time periods may not represent a full climatology. Third, the climate change signal may be weak over the relatively short time span discussed herein (1990-2001 to 2030-2041). This interval between temporal windows was chosen to reflect what we consider to be a reasonable temporal horizon for the majority of individuals involved in impact analysis and mitigation. Finally, it should be emphasized that the findings documented herein were specifically based on simulations conducted using a single a single emission scenario (SRES A2). Just as the results could differ for other periods, they may also differ if another emission scenario were used.

Despite these caveats, our study indicates that before being used to derive regional climate change prognoses, large scale GCM simulations should be tested to ensure that the GCM-simulated synoptic climate is consistent with observations.

6. ACKNOWLEDGEMENTS

This research was supported in part by the Office of Science (BER), U.S. Department of Energy, through the Midwestern Regional Center of the National Institute for Global Environmental Change under Cooperative Agreement No. DE-FC03-90ER61010 via a grant to Pryor, Barthelmie and Carreiro. HadCM3 data has been supplied by the Climate Impacts LINK Project (DERFA Contract EPG 1/1/124) on behalf of the Hadley Centre and U.K. Meteorological Office. JS also gratefully acknowledges a Dissertation Year Research Fellowship from Indiana University.

7. REFERENCES

Blair D (1998) The Kirchhofer technique of synoptic typing revisited. Int J Climatol 18: 1625-1635.

Coleman JS, Rogers JC (2003) Ohio River Valley moisture conditions associated with the Pacific-North American teleconnection pattern. J Climate 16: 969-981.

Dickson RR, Namias J (1976) North American influences on the circulation and climate of the North Atlantic sector. Mon Weather Rev 104: 1255-1265.

Flato GM, Boer, GJ, Lee WG, McFarlane NA, Ramsden D, Reader MC, Weaver AJ (2000) The Canadian Centre for Climate Modeling and Analysis coupled model and its climate. Clim Dynam 16: 451-467.

Flato GM, Boer GJ (2001) Warming asymmetry in climate change simulations. Geophys Res Lett 28: 195-198.

Gordon C, Cooper C, Senior CA, Banks H, Gregory JM, Johns TC, Mitchell JFB, Wood RA (2000) The simulation of SST, sea ice extents and ocean heat transports in a version of the Hadley Centre coupled model without flux adjustments. Clim Dynam 16: 147-168.

Henderson KG, Robinson PJ (1994) Relationships between the Pacific/North American teleconnection patterns and precipitation events in the south-eastern USA. Int J Climatol 14: 307-323.

Hurrell JW, Kushnir Y, Ottersen G, Visbeck M (eds) (2003) The North Atlantic Oscillation: Climatic Significance and Environmental Impact. Washington DC: American Geophysical Union, Geophysical Monograph Series 134, 279pp.

IPCC (2000) Special Report on Emissions Scenarios. Cambridge: Cambridge University Press, 612pp.

Kalnay E, Kanamitsu M, Kistler R, Collins W, Deaven D, Gandin L, Iredell M, Saha S, White G, Woollen J, Zhu Y, Chelliah M, Ebisuzaki W, Higgins W, Janowiak J, Mo KC, Ropelweski C, Wang J, Leetmaa A, Reynolds R, Jenne R, Joseph D (1996) The NCEP/NCAR 40 reanalysis project. B Am Meteorol Soc 77: 437-471.

Kang L-S, Jin K, Lau K-M, Shukla J, Krishnamurthy V, Schubert SD, Waliser DE, Stern WF, Satyan V, Kitoh A, Meehl GA, Kanamitsu M, Galin VYa, Sumi A, Wu G, Liu Y, Kim, J-K (2002) Intercomparison of atmospheric GCM simulated anomalies associated with the 1997-98 El Niño. J Climate 15, 2791-2805.

Katzfey JJ, McInnes KL (1996) GCM simulations of eastern Australian cut-off lows. *Journal of Climate* 9: 2337-2355.

Kirchhofer W (1974) Classification of European 500 mb patterns. Schwiezerische Meteorologische Anstalt, Institut Suisse de Meteorologie, Zurich 43: 1-16.

Kistler R, Kalnay E, Collins W, Saha S, White G, Woollen J, Chelliah M, Ebisuzaki W, Kanamitsu M, Kousky V, van den Dool H, Jenne R, Fiorino M (2001) The NCEP-NCAR 50 year reanalysis: Monthly mean CD-ROM and documentation B Am Meteorol Soc 82: 247-267.

Lamb PJ, Peppler RA (1987) North Atlantic Oscillation: concept and an application. B Am Meteorol Soc 68: 1218-1225.

Lapp S, Byrne J, Kienzle S, Townshend I (2002) Linking global circulation model synoptics and precipitation for western North America. Int J Climatol 22: 1807-1817.

Leathers DJ, Yarnal B, Palecki MA (1991) The Pacific/North American teleconnection pattern and United States climate. Part 1: Regional temperature and precipitation associations. J Climate 4: 517-528.

McKendry IG, Steyn DG, McBean G (1995) Validation of synoptic circulation patterns simulated by the Canadian Climate Centre general circulation model for western North America. Atmos Ocean 33: 809-825.

Osborn TJ, Briffa KR, Tett SFB, Jones PD (1999) Evaluation of the North Atlantic Oscillation as simulated by a coupled climate model. Clim Dynam 15: 685-702.

Ott RL (1993) An Introduction to Statistical Methods and Data Analysis, 4th Edition. Belmont: Duxbury Press, 1051 pp.

Pan Z, Christensen J, Arritt RW, Gutowski W, Takle ES, Otieno F (2001) Evaluation of uncertainties in regional climate change simulations. J Geophys Res-Atmos 106: 17735-17751.

Pope VD, Gallani ML, Rowntree PR, Stratton RA (2000) The impact of new physical parameterizations in the Hadley Centre climate model: HadAM3. Clim Dynam 16: 123-146.

Pryor SC, Barthelmie RJ (2003) Long term trends in near surface flow over the Baltic. Int J Climatol 23: 271-289.

Renshaw AC, Rowell DP, Folland CK (1998) Wintertime low-frequency weather variability in the North Pacific-American sector 1949-93. J Climate 11: 1073-1093.

Satterthwaite FW (1946) An approximate distribution of estimates of variance components. Biometrics Bull 2: 110-114.

Schubert S (1998) Downscaling local extreme temperature changes in south-eastern Australia from the CSIRO Mark2 GCM. Int J Climatol 18: 1419-1438.

Sheridan SC (2003) North American weather-type frequency and teleconnection indices. Int J Climatol 23: 27-45.

Stephenson DB, Pavan V (2003) The North Atlantic Oscillation in coupled climate models: a CMIP1 evaluation. Clim Dynam 20: 381-399.

USNA (2001) Climate Change Impacts on the United States: The Potential Consequences of Climate Variability and Change. Cambridge, 2001.

Wallace JM, Gutzler DS (1981) Teleconnections in the geopotential height field during the Northern Hemisphere Winter. Mon Weather Rev 109: 784-812.

Wilby RL, Wigley TML, Conway D, Jones PD, Hewitson BC, Main J, Wilks DS (1998) Statistical downscaling of general circulation model output: a comparison of methods, Water Resour Res 34: 2995-3008.

Wilks D (1995) Statistical Methods in the Atmospheric Sciences, International Geophysics Series, San Diego: Academic Press, 467 pp.

Willmott CJ (1987) Synoptic weather map classification: correlation versus sums-of-squares. Prof Geogr 39: 205-207.

Yarnal B (1985) A 500 mb synoptic climatology of Pacific North-west Coast winters in relation to climatic variability, 1948-49 to 1977-78. J Climatol 5: 237-252.

Yarnal B, Leathers DJ (1988) Relationships between interdecadal and interannual climatic variations and their effect on Pennsylvania climate. Ann Assoc Amer Geogr 78: 624-641.

Yin Z-Y (1994) Moisture conditions in the south-eastern USA and teleconnection patterns. Int J Climatol 14: 947-967.